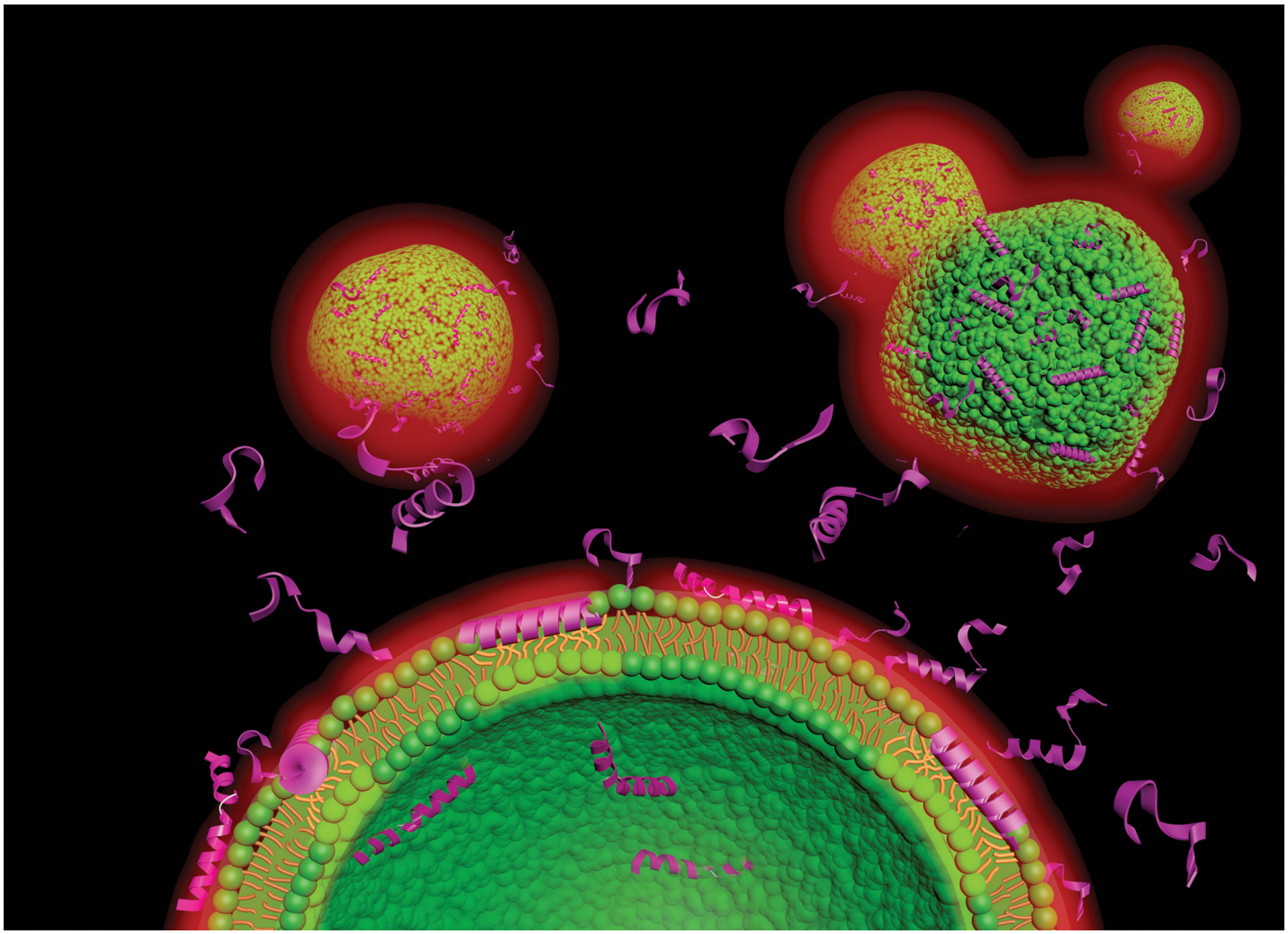

Showcasing research from the Bio-Scattering group of Professor U-Ser Jeng, National Synchrotron Radiation Research Center, Taiwan

Interplay of entropy and enthalpy in peptide binding to zwitterionic phospholipid membranes as revealed from membrane thinning

This work investigates the structure and binding thermodynamics of melittin-bound, phosphocholine-based unilamellar vesicles, on the basis of the membrane thinning observed using small-angle X-ray scattering and diffraction. The peptide binding induces asymmetric bilayer thinning of the vesicle, which can be significantly enhanced with compound thermal thinning at elevated temperatures. Binding isotherms are established from the X-ray results to provide the temperature-dependent binding constant and changes of enthalpy and entropy, which conclude an entropy-driven binding process prior to membrane pore formation.

As featured in:

See Chun-Jen Su, U-Ser Jeng *et al.*, *Phys. Chem. Chem. Phys.*, 2018, **20**, 26830.

ROYAL SOCIETY OF CHEMISTRY

rsc.li/pccp

Registered charity number: 207890

PCCP

PAPER

View Article Online
View Journal | View Issue

Published on 07 August 2018. Downloaded by National Synchrotron Radiation Research on 1/21/2019 4:29:58 AM.

Check for updates

Cite this: *Phys. Chem. Chem. Phys.*, 2018, **20**, 26830

Interplay of entropy and enthalpy in peptide binding to zwitterionic phospholipid membranes as revealed from membrane thinning†

Chun-Jen Su, *[a] Ming-Tao Lee,[a] Kuei-Fen Liao,[a] Orion Shih [a] and U-Ser Jeng *[ab]

Received 5th May 2018,
Accepted 6th August 2018

DOI: 10.1039/c8cp02861c

rsc.li/pccp

Membrane thinning that resulted from peptide-binding is observed *via* temperature dependent small-angle X-ray scattering (SAXS). The result reveals a mean thermal thinning rate of 0.038 Å K^{-1} for the neat unilamellar vesicles (ULVs) of a zwitterionic phospholipid of 1,2-dieicosenoyl-*sn-glycero*-3-phosphocholine (diC20:1PC) in the temperature range of 285–312 K. The thinning effect promotes greatly the association between a model antimicrobial peptide melittin and the ULV. Scaling the observed isothermal melittin–ULV bilayer thinning to that measured using low-angle X-ray diffraction from the melittin–multilamellar membranes of defined peptide-to-lipid ratios establishes temperature-dependent binding isotherms χ_b of the peptide–ULV as a function of free peptide concentration in solution. From the binding isotherms, temperature-dependent peptide–membrane binding constant $K(T)$ is extracted on the basis of a modified Gouy–Chapman model. Changes in $K(T)$ follow the linearized van't Hoff equation $\ln K(T) \propto -\Delta H T^{-1}$ with a constant enthalpy change ΔH = 9.6 kcal mol^{-1}, suggesting an entropy-driven binding process prior to membrane pore formation. Correspondingly, a five-fold enhancement of K is observed in the temperature range studied. The peptide-binding strength is found to follow the growth trend of the membrane thermal thinning rate better than the lipid chain length of the three phosphocholine-based ULVs of diC_n:1PC with n = 18, 20, and 22.

1. Introduction

Direct membrane–peptide interactions are involved in numerous crucial biological processes, such as antimicrobial defense, viral translocation, functioning of membrane proteins, membrane fusion, and transport of therapeutic compounds.[1] The associated peptide activities have attracted great attention in recent years because of their potential biomedical applications.[2,3] For example, antimicrobial peptides (AMPs) have been used as alternatives to traditional antibiotics and fungicides for reduction in drug resistance.[2,3] Most of the AMPs are composed of L-amino acids, which can change their secondary structures to linear, α-helix, and/or β-sheet, prior to or during their interactions with membranes.[2,3] Previous studies have already shown that peptide–lipid interactions can lead to transmembrane pores in cell membranes or mimic membranes of lipid vesicles;[4–8] the corresponding molecular understanding of the dynamic process of membrane structural changes with peptide binding also increases cumulatively with the advance in structural probing methodology.[9–12] Observing membrane structural evolution on a molecular level can provide direct information on the association of peptides with membranes and the related pore formation mechanism, which are crucial factors for therapeutic applications.

Most of the peptide–membrane interactions share a common early stage of membrane partitioning of peptides.[13] During this early stage, binding of peptides to membranes is suggested to be governed by the interplay between enthalpy and entropy.[14] Although charge interactions can attract peptides near charged lipid membranes, hydrophobic interactions between the peptides and membrane lipids are considered as the major driving force of membrane partition of peptides;[15,16] the entropy-driven mechanism, however, is suggested to be dominant when the membrane lipids are well-packed.[14] Elucidating such an interplay between the entropy and enthalpy of peptide–membrane associations under a thermal equilibrium with free peptides in solution requires integrated structural probes.[7,12] Fluorescence and circular dichroism spectroscopies have been widely used in determining the approximate position and orientation of peptides on membranes.[7,12,17] Isothermal calorimetry (ITC)

[a] *National Synchrotron Radiation Research Center, Hsinchu Science Park, Hsinchu 30076, Taiwan. E-mail: su.cj@nsrrc.org.tw, usjeng@nsrrc.org.tw*
[b] *Department of Chemical Engineering, National Tsing Hua University, Hsinchu 30013, Taiwan*

† Electronic supplementary information (ESI) available. See DOI: 10.1039/c8cp02861c

This journal is © the Owner Societies 2018

Published on 07 August 2018. Downloaded by National Synchrotron Radiation Research on 1/21/2019 4:29:58 AM.

allows identification of the changes in thermodynamic properties of the membrane bilayers upon peptide binding.[17] These methodologies together have contributed to the establishment of binding isotherms that give quantitative descriptions of the interactions between AMPs and membranes in solution based on the structural changes of the peptides. Nevertheless, peptide structural changes may occur near the membrane surfaces, and not necessarily coincide with the membrane structural changes upon peptide adsorption.

Delicate structural changes of membranes induced by peptide binding have been probed successfully using low-angle X-ray diffraction (XRD) with substrate-oriented multilamellar membranes (MLMs) premixed with peptides.[7,12,18] Complementarily, solution small-angle X-ray and neutron scattering (SAXS and SANS) with phospholipid unilamellar vesicles (ULVs) has been applied to reveal the membrane structural changes due to peptide binding in solution.[18–23] Moreover, membrane stiffening upon extensive formation of peptide-induced pores was unveiled using neutron spin-echo spectroscopy.[24] In a previous report,[25] we pioneered an integrated approach by SAXS and low-angle XRD to associate the membrane thinning behaviors of ULVs and MLMs of zwitterionic phospholipids upon peptide binding, and establish the binding isotherm of peptides to ULVs.

In this study, we show that the binding affinity of a model peptide melittin to zwitterionic phospholipid ULVs can be enhanced significantly at elevated temperatures owing to thermally enhanced membrane thinning. With combined analysis of SAXS and low-angle XRD, temperature-dependent binding isotherms are established. On the basis of a modified Gouy–Chapman (GC) model,[26] we further extract the temperature-dependent binding constants and effective charge of the adsorbed peptide, from which, the respective contributions of entropy and enthalpy in the peptide–membrane associations are determined quantitatively. The thermodynamics parameters extracted from membrane thinning cover peptide adsorption behavior at high free peptide concentrations (in the order of mM) in solution prior to formation of steady membrane pores. Such information is complementary to that given by optical spectroscopy or the ITC method in a different interaction regime with dilute peptide concentration.

2. Experimental

2.1. Materials and sample preparation

Melittin (93% pure, HPLC grade) (product no. M-2272) and zwitterionic phospholipid 1,2-dieicosenoyl-*sn-glycero*-3-phosphocholine (diC20:1PC) were purchased from Sigma-Aldrich Chemical Co. and Avanti Polar Lipids Inc., respectively. All materials were used as received without further purification. Preparation of ULVs followed the procedure described previously.[25] The mean size of the ULVs determined by dynamic light scattering (Malvern Zetasizer Nano S90) was *ca.* 55 nm, much larger than the bilayer thickness of *ca.* 4 nm. The aqueous solutions of 30–60 mM ULV and 10 mM NaCl were mixed with a 2 or 4 mM melittin solution for various peptide-to-lipid (P/L) molar ratios of up to 0.04 prior to SAXS measurements.

2.2. SAXS measurements

SAXS data were collected at the 23A SWAXS beamline of the Taiwan Light Source of the National Synchrotron Radiation Research Center (NSRRC).[27] Sample solutions were, respectively, loaded in solution cells of 5 mm X-ray path length sealed with thin (30 μm) quartz windows, and measured with a 15 keV beam at 12.5, 20, 30, and 38.5 °C. Instrument calibration and data reduction followed the procedures reported previously for absolute scattering intensity (scattering cross-section per unit volume in units of cm^{-1}).[27]

2.3. SAXS data analysis

SAXS intensity profiles $I(q)$ were modeled using the form factor $I(q) \propto \langle F(q)^2 \rangle$ of unilamellar vesicles,[28] with the scatter vector $q = 4\pi\lambda^{-1}\sin\theta$ defined by the scattering angle 2θ and wavelength λ. The corresponding electron density profile $\rho(r)$[28–30] of the lipid-bilayer form factor is approximated by three Gaussian functions representing the low-electron-density region of aliphatic chains sandwiched by the two high-electron-density regions of headgroups of phospholipids. The hence reconstructed electron density profile for a bilayer of inner and outer leaflets can be symmetric or asymmetric.[28] The scattering form factor Fourier transformed from the electron density profile $\rho(r)$ of the bilayer is

$$F(q) = 2q^{-1}\sum_{k=1}^{3}\rho_k\sigma_k\exp\left(-q^2\sigma_k^2/2\right)\left[\varepsilon_k\sin(q\varepsilon_k) + \sigma_k^2 q\cos(q\varepsilon_k)\right] \quad (1)$$

Here, ρ_k is the amplitude of the kth Gaussian function (in relative electron density), and σ_k and ε_k are the corresponding Gaussian distribution width and displacement from the bilayer center ($r = 0$), as that defined in a previous report.[28]

3. Results and discussion

3.1. Asymmetric lipid bilayer thinning upon melittin binding

Fig. 1a shows the SAXS profiles obtained for the solutions of the mixed diC20:1PC ULV and melittin for the P/L ratios indicated. The second humps of these SAXS curves shift towards the higher q region as P/L increases. The shifting behavior results from the effects of peptide-induced membrane thinning, as observed in a previous study of the diC22:1PC ULV upon melittin binding.[25] Using eqn (1), we could fit the data decently with the $\rho(r)$ profiles shown in Fig. (1b). The increasingly asymmetric $\rho(r)$ profiles as P/L increases represent more asymmetric bilayer leaflets owing to more asymmetric melittin binding from the solution to the outer leaflet of the ULV,[25] resulting in higher $\rho(r)$ peak values than the inner leaflet. As illustrated in Fig. 1c, the increased $\rho(r)$ of the outer leaflet may partly come from the compact binding between the hydrophilic part of the melittin and the phosphate lipid heads. The hydrophobic part of melittin, however, causes local stress of nearby lipid chains for asymmetric fluctuations maximized at the opposite sides of the peptide binding sites (*cf.* Fig. 1c), leading to a broadened $\rho(r)$ peak as in Fig. 1(b).

Published on 07 August 2018. Downloaded by National Synchrotron Radiation Research on 1/21/2019 4:29:58 AM.

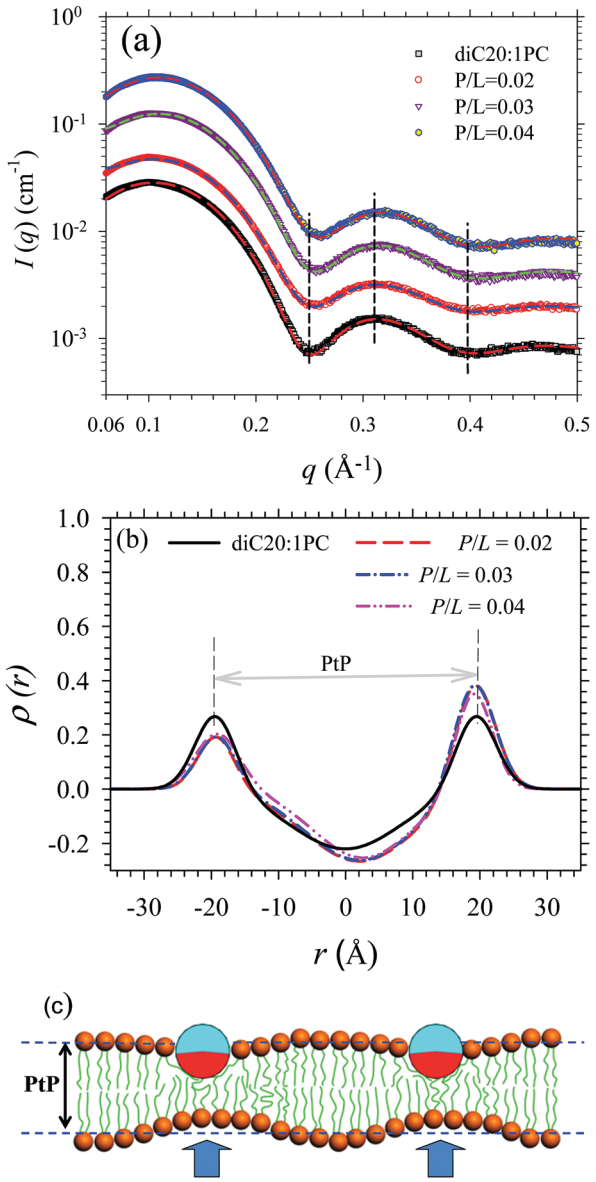

Fig. 1 (a) SAXS profiles for aqueous solutions of diC20:1PC unilamellar vesicles, mixed with melittin for *P/L* ratios of 0.02, 0.03, and 0.04, indicated. The three dashed lines outline the shifting of the broad hump. The data are fitted (dashed curves) using the corresponding bilayer electron density profiles in (b). The arrow in (b) marks the peak-to-peak (PtP) distance of the neat symmetric ULV bilayers. (c) Illustration for an asymmetric peptide binding onto the outer leaflet of the ULV bilayer. The blue and red parts of the circles represent the hydrophilic and hydrophobic cross-section projections of the rod-like melittin.

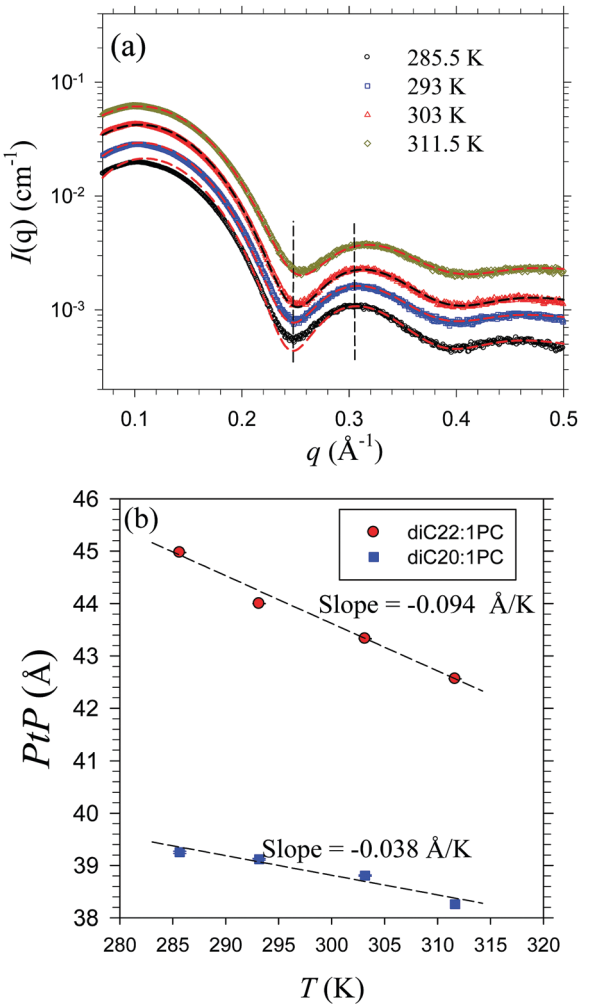

Fig. 2 (a) Temperature dependent SAXS profiles for the diC20:1PC ULV fitted (dashed curves) using symmetric $\rho(r)$ profiles. (b) Corresponding PtP values extracted from the $\rho(r)$ profiles. Also shown are the temperature dependent PtP values of diC22:1PC and diC20:1PC ULVs, linearly fitted with the marked slopes (in units of Å K^{-1}) for the bilayer thermal thinning rates.

3.2. Temperature-dependent symmetric thinning of ULV bilayers

Fig. 2a shows the temperature-dependent SAXS profiles obtained for the ULV of diC20:1PC, exhibiting three clearly discernible humps of the ULV form factor scattering. The second humps of these SAXS curves also shift systematically towards the higher-q region upon increasing the temperature, revealing a decrease in bilayer thickness. In contrast to the melittin-induced asymmetric bilayer thinning, the data can be fitted (Fig. 2a) using symmetric bilayer $\rho(r)$ profiles with a systematically reduced peak-to-peak (PtP) distance of $\rho(r)$ of the ULV bilayers (Fig. S1, ESI†),[23] from which a mean thermal thinning rate $R = -0.038 \pm 0.007$ Å K^{-1} is deduced for diC20:1PC (Fig. 2b). Previous studies[29,30] have shown a general membrane thinning effect of phosphatidylcholine lipid bilayers upon an increase of temperature, owing to the increase in chain disorder. The thickness thinning is accompanied by an increase in area-per-lipid of the bilayers to conserve the lipid volume.[30] For comparison, we have also measured diC22:1PC (1,2-dierucoyl-*sn-glycero*-3-phosphocholine) vesicle bilayers (Fig. S2, ESI†), which yielded a larger $R = -0.094 \pm 0.005$ Å K^{-1} (Fig. 2b) due to the amplified effect of chain disorder with the increased lipid chain length. The smaller thermal thinning rate of the vesicle bilayers of diC20:1PC reveals a better thermal stability. Below, we show that a better thermal stability would lead to a lower peptide binding affinity. We note that the two small thinning rates of diC20:1PC and diC22:1PC

 This journal is © the Owner Societies 2018

Published on 07 August 2018. Downloaded by National Synchrotron Radiation Research on 1/21/2019 4:29:58 AM.

are obtained by fitting the changes in PtP values measured in the temperature range of 285–312 K with an assumed linear relationship. Limited by the uncertainties of the thinning rates hence obtained (Fig. 2b), the distinguishable PtP change in the temperature region is *ca.* 0.2 Å in our measurements. For a reliability check of the SAXS model fitting, the thicknesses of the aliphatic chain zone, 32 ± 1 and 37 ± 1 Å, obtained here for the neat ULVs of diC20:1PC and diC22:1PC at 30 °C (*cf.* Fig. S1 and S2b, ESI†) are consistent with the literature values (32 and 36.6 Å).[31]

3.3. Peptide–membrane binding isotherm

Fig. 3 shows the relative changes in PtP, Δ_{PtP}, for melittin–ULV and melittin–MLM bilayers, respectively, normalized by the PtP values of pure ULV and MLM bilayers of diC20:1PC. With the same peptide–lipid compositions in these two systems, the value of Δ_{PtP} for the peptide–ULV, $(\Delta_{PtP})_{ULV}$, is always smaller than that of the peptide–MLM, $(\Delta_{PtP})_{MLM}$, due to limited peptide binding affinity to the ULV in solution. As there is a little excess water phase for free peptides in the MLM, all the peptides mixed into the MLM system are assumed to be associated with membranes for MLM bilayer thinning observed, namely the bound-peptide-to-lipid molar ratio of MLM $\chi_{MLM} = P/L$.[12] Previous studies have established that MLM thinning is linearly proportional (f) to χ_{MLM}, *i.e.* $(\Delta_{PtP})_{MLM} = f\chi_{MLM}$, when it is away from the critical P/L^* for membrane pore formation.[12] In this linear thinning regime, the adsorbed melittin forms a helical conformation and orients parallel to the plane of the bilayers.[7,12]

Following a previous analysis,[25] the dimensionless thinning constant $f = (\Delta_{PtP})_{MLM}/\chi_{MLM} = -2.6 \pm 0.1$ is fitted from the linear bilayer thinning data of melittin-bound MLM of diC20:1PC (Fig. 3). Previously, we have shown that ULV and MLM phospholipid bilayers share a common peptide-thinning constant based on the alamethicin–diC22:1PC system.[25] Using the f constant we

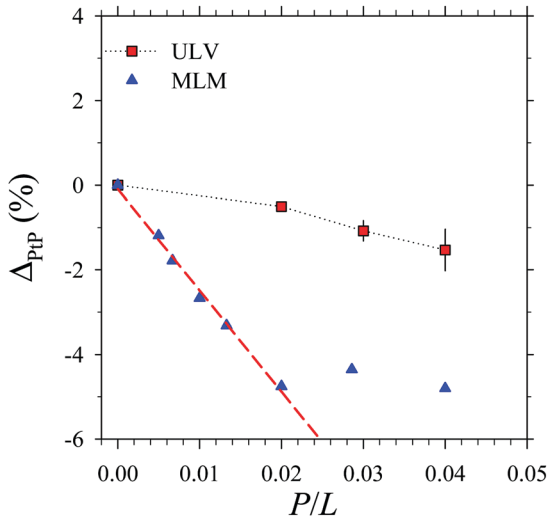

Fig. 3 Relative changes in PtP, Δ_{PtP}, for the melittin-bound ULV and MLM of diC20:1PC *vs.* the peptide–lipid ratio P/L of the systems. The Δ_{PtP} values for the MLM before saturation are linearly fitted (dashed line with slope f). The MLM data were adapted from a previous report.[12]

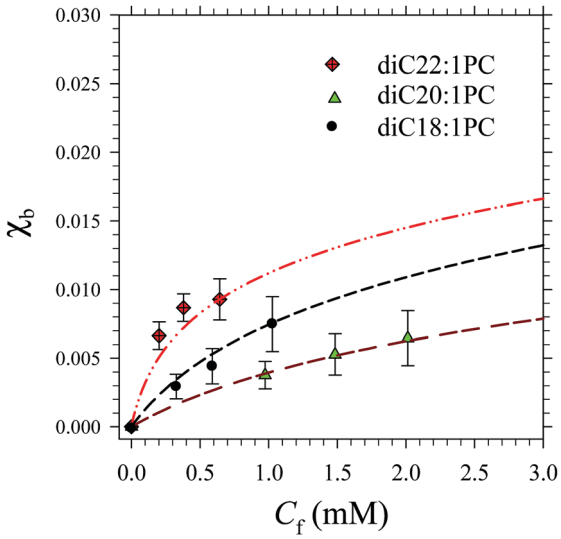

Fig. 4 Peptide-to-lipid binding ratio, χ_b, of the melittin-bound diC20:1PC ULV, as a function of free peptide concentration C_f in the solution. The melittin binding isotherms with diC22:1PC and diC18:1PC ULVs are also shown. The data are fitted (dashed curves) using a modified GC model.

can deduce the bound peptide–lipid molar ratio $\chi_b = (\Delta_{PtP})_{ULV}/f$ for the melittin-bound ULV bilayers from the ULV thinning result, and establish a binding isotherm as a function of free peptide concentration C_f in solution. Here, C_f is deduced by subtracting the membrane-bound peptide concentration from the total peptide concentration.[25] Fig. 4 shows the binding isotherm thus converted from the $(\Delta_{PtP})_{ULV}$ data in Fig. 3. We note that the binding isotherm is established on the basis of membrane thinning upon peptide binding, which is complementary to those obtained from the changes in the peptide conformation.[17]

We further use a modified Gouy–Chapman model[32] to quantitatively correlate the peptide adsorption with the free peptide concentration in solution and surface charge of the lipid bilayers. According to the model, the equilibrium χ_b is correlated with C_f *via* a binding constant K (*i.e.* the surface partition constant) in the form of

$$\chi_b = KC_f \exp(-z_p e_0 F\Psi_0/RT) \quad (2)$$

with the effective peptide charge number z_p, units of elementary charge e_0, Faraday constant F, and thermal energy RT. The charge potential $\Psi_0(\chi_b, z_p)$ built from melittin adsorption onto the membranes saturates with an equilibrium peptide concentration immediately above the lipid membrane $C_m = C_f \exp(-z_p e_0 F\Psi_0/RT)$, which is defined as the surface partition equilibrium.

In the modified GC model, the membrane surface charge density σ reaches equilibrium with the electrolytes in the solution for

$$\sigma^2 = \sum_i \alpha c_i [\exp(-z_i e_0 F\Psi_0/RT) - 1] \quad (3)$$

where $\alpha = 2000\,\varepsilon_0\varepsilon_R RT$ with ε_0 the permittivity of free space and ε_R the dielectric constant of water; c_i and z_i are, respectively, the concentration and charge number of the ith electrolyte (10 mM NaCl in our case) in the bulk aqueous phase. Moreover, the

Published on 07 August 2018. Downloaded by National Synchrotron Radiation Research on 1/21/2019 4:29:58 AM.

mean membrane surface charge density may be defined by the number of net charge per lipid area absorbed with χ_b peptide

$$\sigma = z_p\chi_b/(A_L + A_p\chi_b) \quad (4)$$

for zwitterionic phospholipid membranes. The lipid head area A_L is approximated by $A_{L0}(1 + \chi_b)$ (which increases roughly linearly with χ_b due to the approximately linear thinning of the bilayer thickness), with A_{L0} = 71.5 Å^2 averaged from 69 Å^2 and 74 Å^2 reported, respectively, for diC22:1PC and diC18:1PC.[12,20,23,33] The cross section area A_p = 241.5 Å^2 of melittin (in a parallel-to-membrane adsorption state; *cf.* Fig. 1c) used in the fitting process is an average of the reported values of 237 and 246 Å^2 for the melittin-adsorbed MLM of diC22:1PC and diC18:1PC, respectively.[33,34] With eqn (2)–(4), we can derive an iteration relation of χ_b in the form of

$$\chi_b = KC_f\left[(\beta + 2) + \frac{(\beta^2 + 4\beta)^{1/2}}{2}\right]^{-z_p} \quad (5)$$

with $\beta = [z_p e_0\chi_b/(A_L + A_pX_b)]^2/\alpha c$ (with monovalent electrolyte $c = c_i$). As β is also a function of χ_b, eqn (5) is rearranged into

$$C_f = \frac{\chi_b}{K}\left[(\beta + 2) + \frac{(\beta^2 + 4\beta)^{1/2}}{2}\right]^{z_p} \quad (6)$$

for practical data fitting with the two fitting parameters, K and z_p. With the fitted K and z_p values, we then recalculate the simulation curves $\chi_b(C_f)$ using eqn (5) as shown in Fig. 4. Previous reports suggested that z_p is always smaller than the physical valency of membrane-adsorbed peptides due to the finite size and discrete charge effects of the adsorbed peptides (note that melittin has six charged side chains).[31,35] In Fig. 4, the SAXS-determined binding isotherm of melittin to diC20:1PC is fitted decently with K = 6.8 ± 0.2 M^{-1} and z_p = 1.8 ± 0.6, using eqn (6). The fitted z_p value supports a theoretical prediction of z_p = 2.2 reported previously for melittin in solutions of 10 mM ionic strength.[35] For a consistency check of the modified GC model, we have further established the binding isotherms of melittin to diC22:1PC (with f = −3.0) and diC18:1PC (1,2-dioleoyl-*snglycero*-3-phosphocholine or DOPC) with f = −2.5, using the measured SAXS data shown in Fig. S3, ESI,† and the low-angle X-ray diffraction data in the literature.[12,18] Both the binding isotherms can also be fitted with the same z_p = 1.8, together with significantly larger K values of 53.8 ± 7 and 16.1 ± 2 M^{-1}, respectively, for diC22:1PC and diC18:1PC ULVs at 303 K, as that shown in Fig. 4 and Table 1. We notice that the diC20:1PC ULV has the smallest K value compared to diC22:1PC and diC18:1PC ULVs. Interestingly, these binding K values do not increase with the increase of the chain length of the ULV lipids. Instead, they increase with the increase of the membrane thermal thinning rates of R = −0.038, −0.051, and −0.090 Å K^{-1}, respectively, for diC20:1PC, diC18:1PC,[20] and diC22:1PC ULVs (*cf.* Fig. 2b). Since a higher thinning rate corresponds to larger entropy gain, the result implies that melittin's partitioning into these bilayers is an entropy-dominated process.

Table 1 Temperature dependent binding constant $K(T)$ of melittin to the ULV of diC20:1PC. Also shown are the K values with diC18:1PC and diC20:1PC vesicle bilayers measured at 303 K

Melittin	K (M^{-1}) 285.5 K	K (M^{-1}) 293 K	K (M^{-1}) 303 K	K (M^{-1}) 311.5 K
diC18:1PC			16.1 ± 2.0	
diC20:1PC	1.9 ± 0.2	4.3 ± 0.5	6.8 ± 0.2	9.1 ± 0.2
diC22:1PC			53.8 ± 7.0	

Previous studies have established that the lipid volume in a bilayer remains nearly constant during temperature changes far from lipid phase transitions.[36,37] With conservation of the lipid volume, percentage changes in the area per lipid and aliphatic zone thickness h of the ULV bilayers are correlated *via* $\delta A_L/A_L = -\delta h/h$.[37] Therefore, one would expect a higher thermal thinning rate with longer chain length in these lipids of a homologous headgroup. Our results, however, reveal that the diC20:1PC ULV bilayer behaves unexpectedly, with a thinning rate lower than that of the diC18:1PC ULV, which suggests a relatively optimized chain packing that originated from its molecular structure. Presumably, the influence of the cis double bond position of the chain from the head group outweighs that of the chain length in this particular case.[38] Interestingly, our dynamic light scattering results also show the smallest mean size for the diC20:1PC ULV among the three types of ULVs prepared with the same lipid concentration (Fig. S5, ESI†), revealing consistently a relatively strongest chain–chain interaction.[39,40] A previous study[41] also suggested that the positions of the cis double bonds of an unsaturated phospholipid could regulate the interplay between the enthalpy (through chain–chain interactions) and entropy of the lipid in bilayer packing, resulting in non-linear changes in enthalpy and entropy with the chain length. The interplay of the chain packing and entropy is further elucidated below.

3.4. Entropy-driven peptide binding

We have shown that both temperature elevation and peptide-binding induce membrane thinning of diC20:1PC vesicle bilayers. Peptide binding to the membrane surface is, however, driven by the interplay of entropy and enthalpy. The former involves entropy of mixing the peptide, lipids, and water molecules in a bilayer conformation; the latter includes both the electrostatic interactions between the peptide and the membrane and the chain–chain interaction of the membrane lipids. To elucidate the interplay of entropy and enthalpy in the association of melittin with the di20:1PC ULV, we conducted temperature dependent SAXS for the melittin–diC20:1PC ULV in solutions of P/L ratios ranging from 0–0.04 (*cf.* Fig. S4, ESI†). Shown in Fig. 5a are the four sets of thinning behavior of the diC20:1PC vesicle bilayers (represented by the PtP values) at four different temperatures. These results evidence increasingly enhanced membrane thinning at elevated temperatures from 285.5 to 312 K. From these data, we further establish four temperature dependent binding isotherms (Fig. 5b), following the same data analysis procedure shown before. On the basis of the modified GC model and the same z_p = 1.8 obtained previously, the binding isotherms are well fitted (Fig. 5b) with the successively increased $K(T)$ values summarized in Table 1. The result illustrates quantitatively that the melittin binding affinity can be promoted nearly by fivefold in the temperature range.

 This journal is © the Owner Societies 2018

Published on 07 August 2018. Downloaded by National Synchrotron Radiation Research on 1/21/2019 4:29:58 AM.

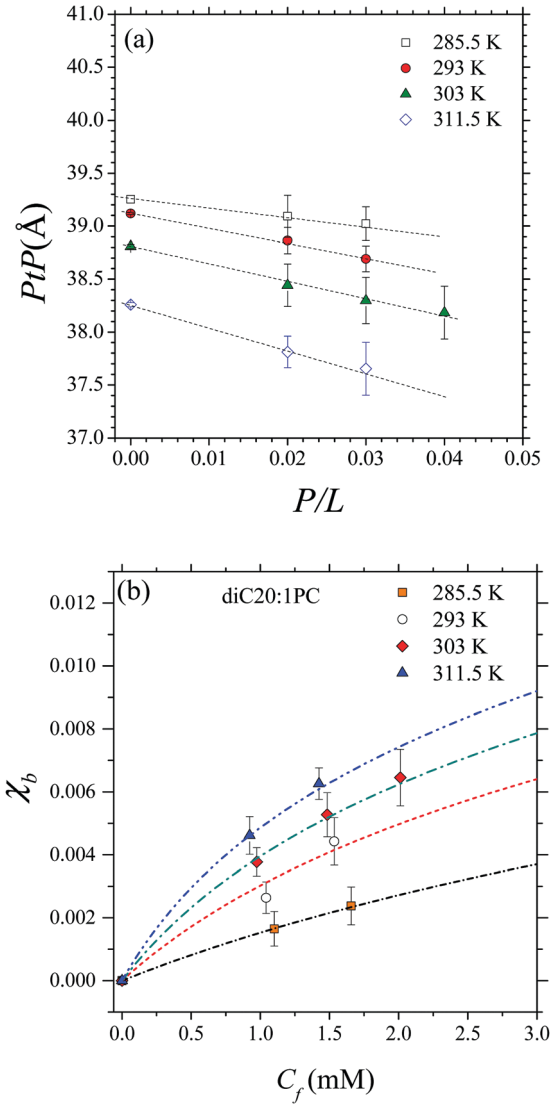

Fig. 5 (a) The changes in PtP values for the melittin-bound ULV of the diC20:1PC ULV with an increase of P/L at the four different temperatures indicated. (b) Corresponding temperature dependent binding isotherms fitted (dashed curves) using a modified GC model.

Previous reports suggest that the change in Gibbs free energy $\Delta G = \Delta H - T\Delta S$ (defined by the changes in enthalpy ΔH and entropy ΔS) upon membrane surface binding of peptides in ideal solution may be approximated by an expression for ideal gas,[42]

$$\Delta G = -RT\ln(55.5 \times K) \quad (7)$$

where the gas constant R = 1.987 cal K^{-1} mol^{-1} and the factor 55.5 corrects for the cratic contribution.[42] Combining eqn (7) with the Gibbs free energy change leads to the linearized van't Hoff expression

$$\ln(K) = -\Delta H/RT + \Delta S'/R \quad (8)$$

with the entropy term $\Delta S'$ convoluted with the cratic contribution. We found that the temperature dependent peptide binding behavior observed (Fig. 6) follows largely the linear relation

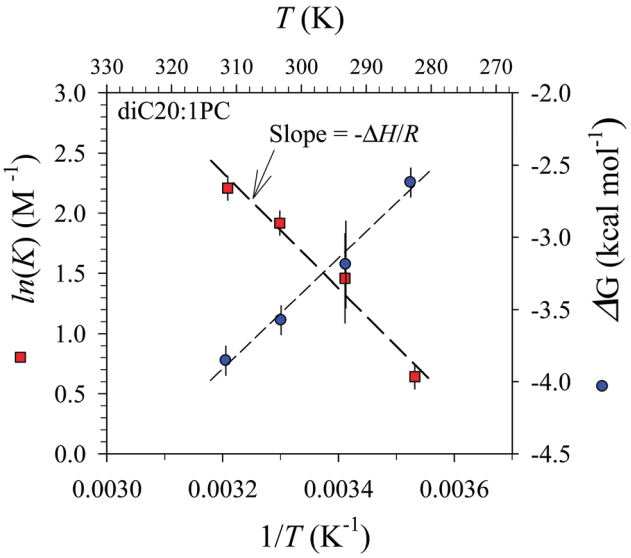

Fig. 6 The binding constant $K(T)$ of melittin to the diC20:1PC ULV and the corresponding Gibbs free energy change $\Delta G(T)$. The $K(T)$ values are linearly fitted (long dashed curves) with the slope $-\Delta H/R$. Note that ΔG is plotted against T (the above X-axis).

of ln(K) with T^{-1} in eqn (8), revealing approximately constant ΔH and $\Delta S'$. The corresponding ΔH = 9.6 ± 1.2 kcal mol^{-1} and $\Delta S'$ = 0.035 ± 0.002 kcal K^{-1} mol^{-1} for melittin's partitioning into the membrane are deduced from the fitted slope and intercept using eqn (8) (Fig. 6). The positive ΔH value indicates that the reduction in ΔG with an increase of temperature shown in Fig. 6 can be attributed mainly to the change in the entropy term for an entropy-driven process of the melittin–membrane association.[43] Traditionally, weak peptide binding to zwitterionic membranes can only be measured at very low peptide concentration in solution *via* optical spectroscopy or ITC, leading to high peptide binding affinities that are not sensitive to temperature changes.[44,45] Here, the peptide–membrane binding thermodynamics parameters at high peptide concentration close to membrane pore formation can be sensitively determined with membrane thinning for the small changes in K values in the temperature range studied (Table 1). Consequently, nearly temperature-independent ΔH and $\Delta S'$ values for melittin's binding to the diC20:1PC ULV could be sensitively determined from the systematic changes in $K(T)$ with temperature. Without systematic changes in $K(T)$, these two terms in a similar melittin–membrane binding were reported to decrease abnormally in absolute values with temperature without justification.[32] In our case with constant values of ΔH and $\Delta S'$, we can further define ΔG = 0 for a critical temperature $T_{sb} = \Delta H/\Delta S'$ = 274 K for spontaneous binding. Above T_{sb}, ΔG becomes negative and decreases linearly with T (Fig. 6) owing to an enlarged $-T\Delta S'$ effect for enhanced partitioning of peptides into a lipid bilayer. We note that the constant ΔH in the range of χ_b observed (Fig. 5b) suggests that, as expected, there should be no change in the melittin–membrane interaction mechanism prior to the critical bound-peptide-to-lipid molar ratio χ_b* (= 0.014 for melittin with diC20:1PC bilayers[12]) for membrane pore formation.

Published on 07 August 2018. Downloaded by National Synchrotron Radiation Research on 1/21/2019 4:29:58 AM.

4. Conclusions

Peptide binding isotherms of phosphocholine-based ULVs in solution are established on the basis of membrane thinning upon melittin binding, using integrated SAXS and low-angle X-ray diffraction. With a modified GC model, temperature-dependent binding constants of melittin to the ULVs are determined together with an effective charge of the membrane-adsorbed melittin. The developed methodology correlates membrane thinning with peptide binding thermodynamics in solution of high peptide concentrations, and can quantify the entropy and enthalpy in the entropy-driven peptide–membrane interactions. Before the critical peptide concentration for membrane pore formation, the peptide–membrane binding affinity studied is proportional to the ULV bilayer thermal thinning rate.

Conflicts of interest

There are no conflicts to declare.

Acknowledgements

The authors are grateful for the elaborated sample preparation by S. S. Wu and W.-Y. Lin. Funding support from the Ministry of Science and Technology, Taiwan (under MOST 105-2112-M-213-010-MY3), is acknowledged.

Notes and references

1 S. Galdiero, A. Falanga, M. Cantisani, M. Vitiello, G. Morelli and M. Galdiero, *Int. J. Mol. Sci.*, 2013, **14**, 18758–18789.
2 H. G. Boman, *Annu. Rev. Immunol.*, 1995, **13**, 61–92.
3 B. Mishra, S. Reiling, D. Zarena and G. Wang, *Curr. Opin. Chem. Biol.*, 2017, **38**, 87–96.
4 M. Zasloff, *Nature*, 2002, **415**, 389–395.
5 H. W. Huang and N. E. Charron, *Q. Rev. Biophys.*, 2017, **50**(e10), 1–17.
6 K. R. Mahendran, A. Niitsu, L. Kong, A. R. Thomson, R. B. Sessions, D. N. Woolfson and H. Bayley, *Nat. Chem.*, 2017, **9**, 411–419.
7 H. W. Huang, F.-Y. Chen and M.-T. Lee, *Phys. Rev. Lett.*, 2004, **92**, 198304.
8 S. M. Hurtley, *Science*, 2005, **310**, 1451.
9 J. Ruan, S. Xia, X. Liu, J. Lieberman and H. Wu, *Nature*, 2018, **557**, 62–67.
10 M.-T. Lee, T.-L. Sun, W.-C. Hung and H. W. Huang, *Proc. Natl. Acad. Sci. U. S. A.*, 2013, **110**, 14243–14248.
11 T. Salditt, C. Li and A. Spaar, *Biochim. Biophys. Acta*, 2006, **1758**, 1483–1498.
12 M.-T. Lee, W.-C. Huang, F.-Y. Chen and H. W. Huang, *Proc. Natl. Acad. Sci. U. S. A.*, 2008, **105**, 5087–5092.
13 S. H. White and W. C. Wimley, *Curr. Opin. Struct. Biol.*, 1994, **4**, 79–86.
14 J. Seelig and P. Ganz, *Biochemistry*, 1991, **30**, 9354–9359.
15 F.-V. Mónica, H. W. Stephen and S. L. Alexey, *J. Membr. Biol.*, 2011, **239**, 5–14.
16 T. Wieprecht, O. Apostolov and J. Seelig, *Biophys. Chem.*, 2000, **85**, 187–198.
17 J. Seelig, *Biochim. Biophys. Acta*, 2004, **1666**, 40–50.
18 F.-Y. Chen, M.-T. Lee and H. W. Huang, *Biophys. J.*, 2003, **84**, 3751–3758.
19 N. Kučerka, J. F. Nagle, J. N. Sachs, S. E. Feller, J. Pencer, A. Jackson and J. Katsaras, *Biophys. J.*, 2008, **95**, 2356–2367.
20 J. Pan, S. Tristram-Nagle, N. Kučerka and J. F. Nagle, *Biophys. J.*, 2008, **94**, 117–124.
21 N. Kučerka, J. Pencer, J. N. Sachs, J. F. Nagle and J. Katsaras, *Langmuir*, 2007, **23**, 1292–1299.
22 N. Kučerka, Y. Liu, N. Chu, H. I. Petrache, S. Tristram-Nagle and J. F. Nagle, *Biophys. J.*, 2005, **88**, 2626–2637.
23 J. Pan, D. P. Tieleman, J. F. Nagle, N. Kucerka and S. Tristram-Nagle, *Biochim. Biophys. Acta*, 2009, **1788**, 1387–1397.
24 J.-H. Lee, S.-M. Choi, C. Doe, A. Faraone, P. A. Pincus and S. R. Kline, *Phys. Rev. Lett.*, 2010, **105**, 038101.
25 C.-J. Su, S.-S. Wu, U. Jeng, M.-T. Lee, A.-C. Su, K.-F. Liao, W.-Y. Lin, Y.-S. Huang and C.-Y. Chen, *Biochim. Biophys. Acta*, 2013, **1828**, 528–534.
26 D. H. Mengistu, E. E. Kooijman and S. May, *Biochim. Biophys. Acta*, 2011, **1808**, 1985–1992.
27 U. Jeng, C.-H. Su, C.-J. Su, K.-F. Liao, W.-T. Chuang and Y.-H. Lai, *J. Appl. Crystallogr.*, 2010, **43**, 110–121.
28 M. R. Brzustowicz and A. T. Brunger, *Appl. Crystallogr.*, 2005, **38**, 126–131.
29 G. Pabst, M. Rappolt, H. Amenitsch and P. Laggner, *Phys. Rev. E: Stat. Phys., Plasmas, Fluids, Relat. Interdiscip. Top.*, 2000, **62**, 4000–4009.
30 N. Kučerka, M. P. Nieh and J. Katsaras, *Biochim. Biophys. Acta*, 2011, **1808**, 2761–2771.
31 J. Gallová, D. Uhríková, N. Kučerka, J. Teixeira and P. Balgavý, *Biochim. Biophys. Acta*, 2008, **1778**, 2627–2632.
32 T. B. Kinraide, *Plant Physiol.*, 1994, **106**, 1583–1592.
33 H. W. Huang, *Biophys. J.*, 1986, **50**, 1061–1070.
34 H. W. Huang, *Biochim. Biophys. Acta*, 2006, **1758**, 1292–1302.
35 S. Stankowski, *Biophys. J.*, 1991, **60**, 341–351.
36 H. Ebel, P. Grabitz and T. Heimburg, *J. Phys. Chem. B*, 2001, **105**, 7353–7360.
37 O. Shih, Y.-Q. Yeh, K.-F. Liao, C.-J. Su, P.-H. Wu, R. K. Heenan, T.-Y. Yu and U. Jeng, *J. Phys. Chem. Lett.*, 2018, **9**, 4287–4293.
38 C. Huang, D. Quinn, Y. Sadovsky, S. Suresh and K. J. Hsia, *Proc. Natl. Acad. Sci. U. S. A.*, 2017, **114**, 2910–2915.
39 C.-M. Lin, D. T. Wu, H.-K. Tsao and Y.-J. Sheng, *Soft Matter*, 2012, **8**, 6139–6150.
40 C.-M. Lin, C.-S. Li, Y.-J. Sheng, D. T. Wu and H.-K. Tsao, *Langmuir*, 2012, **28**, 689–700.
41 D. Marsh, *Biophys. J.*, 1999, **77**, 953–963.
42 D. Persson, P. E. G. Thorén, M. Hemer, P. Lincoln and B. Nordén, *Biochemistry*, 2003, **42**, 421–429.
43 K. Shintou, M. Nakano, T. Kamo, Y. Kuroda and T. Handa, *Biophys. J.*, 2007, **93**, 3900–3906.
44 G. Klocek, T. Schulthess, Y. Shai and J. Seelig, *Biochemistry*, 2009, **48**, 2586–2596.
45 P. Wessman, A. A. Stromstedt, M. Malmsten and K. Edwards, *Biophys. J.*, 2008, **95**, 4324–4336.

 This journal is © the Owner Societies 2018